ISSN-1996-918X

Pak. J. Anal. Environ. Chem. Vol. 26, No. 2 (2025) 273 – 282

http://doi.org/10.21743/pjaec/2025.12.08

Biosynthesis of Ag-doped ZnO Nanoparticles from Melon Peel Extract and Investigation of Their Antibacterial Activity

Saida Soualmi[1*], Meriem Henni[1], Leila Djahnit[2,3], Chaimaa Djerad[1]

[1]*Laboratory of Synthesis and Catalysis, University of Ibn Khaldoun, Tiaret 14000, Algeria.*

[2]*Chemistry Department, Faculty of Exact Sciences and Informatics, University Hassiba Benbouali Chlef (UHBC), Chlef, 02000 Algeria.*

[3]*Renewable Energy and Materials Laboratory, University of Medea, Medea, 26000 Algeria.*

*Corresponding author Email: saida.soualmi@univ-tiaret.dz

Received 11 December 2024, Revised 20 September 2025, Accepted 29 December 2025

Academic Editor: Aamna Balouch

Abstract

This study was designed to synthesise zinc oxide (ZnO) and silver-doped zinc oxide (ZnO:Ag) nanoparticles using an aqueous extract of melon peels as a natural reducing and stabilising agent. For the first time, melon peel extract was used to produce both pure ZnO and Ag-doped ZnO nanoparticles at doping levels of 2% and 3%. The synthesised nanoparticles were characterised by FTIR, XRD, SEM, and EDX methods. XRD analysis revealed a hexagonal crystal structure in all samples, with crystallite sizes of 28.51 nm (ZnO), 26.06 nm (ZnO:Ag 2%), and 37.96 nm (ZnO:Ag 3%). FTIR results confirmed the incorporation of silver into the ZnO matrix. Scanning electron microscopy (SEM) showed mostly spherical particles, with ZnO:Ag 2% exhibiting well-defined crystallinity. EDX results confirmed the successful doping of ZnO with silver. The synthesis of ZnO:Ag 2% nanoparticles demonstrated significant antibacterial properties against *Staphylococcus aureus, Bacillus cereus,* and *Escherichia coli,* with photocatalysis revealing 85% degradation of methylene blue (MB).

Keywords: Melon peel, ZnO nanoparticles, biosynthesis, photocatalysis, antibacterial activity

Introduction

ZnO nanoparticles have great potential in biological applications such as antibacterials, antifungals, acaricides, and lice [1–4]. Recently, ambient methods for nanoparticle synthesis have gained popularity among researchers because of their low cost, simplicity, and environmental compatibility. Several plant extracts—such as *Parthenium hysterophorus* leaf extract, *Azadirachta indica* (Neem) leaf extract, *Aloe socotrina* leaf extract, *Ziziphus jujube,* and *Punica granatum* peel extract have been used for the synthesis of ZnO NPs by different researchers [5–10].

Among various metal oxide nanoparticles, ZnO NPs have attracted considerable attention due to their wide range of applications. These include antioxidant, antibacterial, and photocatalytic activities [11–13], as well as applications in water treatment and dye degradation [12]. ZnO nanoparticles synthesized using *Bacillus thuringiensis* showed insecticidal properties [14]. The wide bandgap of ZnO is responsible for the need for UV light to excite electrons/holes, which creates a major obstacle in photocatalysis since only about 5% of sunlight is in the UV

range [15]. It is clear from the literature that silver (Ag) appears to be the most effective dopant for improving photocatalytic performance [16–17]. Moreover, these nanoparticles exhibit enhanced antibacterial and antifungal activities [18–19]. Although the biosynthesis of ZnO-doped Ag nanoparticles offers several advantages, there are still challenges that need to be addressed. One major challenge revolves around standardizing the synthesis process, as the influence of biological resources may vary, leading to variations in nanoparticle properties. This work reports the synthesis of ZnO NPs via the green route using aqueous melon peel extract. The ZnO NPs were doped with Ag and evaluated for their antibacterial activity and photocatalytic degradation of methylene blue.

Materials and Methods

Preparation of melon peel aqueous extract

Melon peels were washed and sun-dried. They were then ground into a fine powder. Five grams of the melon peel powder were mixed with distilled water. The mixture was stirred vigorously at 60 °C for 30 min, then filtered. The resulting solution was stored at 4 °C.

Biosynthesis of Zinc Oxide Nanoparticles

In order to synthesize ZnO NPs, a 5 mL aqueous extract of melon peels served as the reducing agent. The precursor solution was meticulously prepared by a 250 mL aqueous zinc acetate solution (0.2 M) with a separate 250 mL solution of NaOH (0.5 M). With vigorous stirring, the NaOH solution was carefully added dropwise to the zinc acetate solution containing melon rind extract, forming a light brown zinc hydroxide precipitate at pH=12. The light brown precipitate was separated by centrifugation and washed three times with water and then with ethanol. The obtained product was dried at 60 °C for 24 hours in an air atmosphere and calcined at 650 °C for 4 hours to obtain ZnO NPs.

Ag-doped ZnO sample synthesis

The Ag-doped ZnO sample was prepared by the sol-gel method. 0.2 M zinc acetate (0.05 mol) and 5 mL of melon peel aqueous extract were dissolved in deionized water (solution 1) and stirred. Silver nitrate was prepared separately by dissolving 0.0015 mol for (Ag:3% ZnO) and 0.001 mol for (Ag:2% ZnO) in a little deionized water (solution 2). After that, solution 2 was added to solution 1 and stirred for 30 min. Then, the NaOH solution was carefully added dropwise to the mixture of the two solutions under continuous stirring until a light gray precipitate at pH 12 was formed, which was separated by centrifugation and then washed three times with water and then with ethanol, dried at 60 °C for 24 hours in an air atmosphere, and calcined at 650 °C for 4 hours.

Bacterial strains and growth conditions

The bacterial strains used were E. coli (*Escherichia coli*) ATCC 25922, S. aureus (*Staphylococcus aureus*) ATCC 25925, and B.Cereus(*Bacillus Cereus*) ATCC 10876, and B.Subtilus (*Bacillus Subtilus*) ATCC 6633. Pathogenic microorganisms were subcultured overnight at 37 °C in Mueller-Hilton Agar and then incubated at 37 °C for 18 h to 24 h. Then, 2 to 3 isolated bacterial colonies were discharged into 9 mL of physiological water (0.9% NaCl) and homogenized using a vortex. A spectrophotometer adjusted the turbidity to 0.5 McFarland at 625 nm. The bacterial suspensions contain approximately 1x108 to 2x108 CFU/mL [20]. The antibacterial activity of ZnO nanoparticles is evaluated

using a well diffusion method according to the protocol described by Aldeen et al. [21] with a small modification. Bacterial cultures were distributed evenly on the surface of the nutrient agar with a sterile swab. Four wells of 8 mm diameter were made using a Pasteur pipette. A volume of 100 µL of increasing concentrations of nanoparticles (2, 5, 8, and 10 mg/mL) was placed in each well. The kneaded dishes were allowed to diffuse for 40 min at a temperature of 4 °C, then incubated at 37 °C for 24 h. The diameters of the inhibition zones were measured and recorded.

Characterization Methods of NPs

Fourier transform infrared spectroscopy of ZnO alone and doped NPs was obtained using an FTIR spectrophotometer FTIR-8400 type SHIMADZU. Diffractometer Rigaku MINIFLEX 600 was used for measurement, X-ray diffraction patterns, Cu Kα radiation source (λ= 1.541Å) in the 2θ range from 20 to 80, and the scanning rate of 5° min^{-1}. Scherrer's equation [22] was used to estimate the crystal's size. Using a scanning electron (SEM- QUANTA 650 FEI) microscope, the surface morphology of the prepared nanoparticles of ZnO doped by 2% Ag was investigated.

Photocatalysis

Applying ZnO NPs in treatment through photocatalytic decomposition was carried out using a methylene blue (MB) dye solution [BM]=10 mg/L, pH=8.5. The photocatalytic experiments were completed in the presence of a light source, Omnilux UV lamp 230V/25W.

The reaction vessel was filled with 50 mL of aqueous MB dye solution, followed by adding 25 mg of photocatalyst (Ag-doped ZnO nanoparticles) at room temperature, and pHzpc=8.448 obtained by the pH drift method. A period of 30 min in the dark was spent stirring the produced solution constantly in order to establish the adsorption/desorption equilibrium between dye and photocatalyst. Later on, the sample solutions were exposed to light irradiation. During the irradiation, a portion of the solution (4 mL) was taken from the photocatalytic reactor every 30 min. Next, centrifugation was utilized for separating the nanoparticles, and finally, the concentration of residual MB dye was estimated with an ultraviolet-visible spectrophotometer at a wavelength of 664 nm, respectively. The percentage degradation efficiency calculation involved the usage of the following formula:

$$\%\ Removal = \frac{100X\ (A_0 - A_t)}{A_0} \qquad (1)$$

Wherein A_o is the initial concentration and $(A)_t$: designates the residual concentration in solution at a specific time (t).

Results and Discussion

Fourier Transform Infrared Spectroscopy

Figure 1A displays the FTIR spectra of the functional groups of the green-synthesised ZnO NPs and ZnO samples doped with Ag. The 500–4000 cm^{-1} range is where the spectra were acquired. The band seen between 400 and 800 cm^{-1} corresponds to the Zn–O stretching mode, providing evidence for the creation of ZnO. This peak is likely due to the interaction and bonding of ZnO NPs with the hydroxyl group, forming Zn–O bonds.

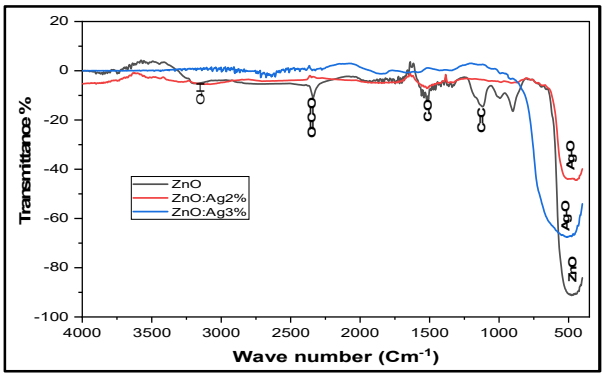

Figure 1A. **FTIR spectrum of (i) ZnO nanoparticles, (ii) ZnO:Ag 2%, and (iii) ZnO:Ag 3% nanoparticles**

Fig. 1A exhibited a wide band at 3459 and 3478 cm^{-1}, which was a consequence of O-H stretch appears in the spectrum can be associated with phenolic and alcoholic compounds. The peaks at 2358 and 2368 cm^{-1} could be associated with the atmospheric CO_2 existing in the environment. The peak shift since 479 cm^{-1} to 536 cm^{-1} for ZnO:Ag 2%, and to 508 cm^{-1} for ZnO:Ag 3% suggests that Ag has been doped into the ZnO host lattice [23].

The peak at 906.5 cm^{-1} corresponds to the stretching vibration of the C-N bond of the primary amine or the C-O bond of the primary alcohol. The peaks at 1011 cm^{-1} are due to bending or vibrations in the plane of secondary alcohols.

X-Ray Diffraction, EDX, and SEM

As illustrated in Fig. 1B, the main significant peaks are located at: 2θ: 31.84°, 34.37°, 36.20°, 47.50°, 56,54°, 62.82°, 66.32°, 67.90°, 69.03°, 72.55°, 76,93 and which are in turn indexed to: (100), (002), (101), (012), (110), (013), (200), (112), (201), (004), (202), respectively.

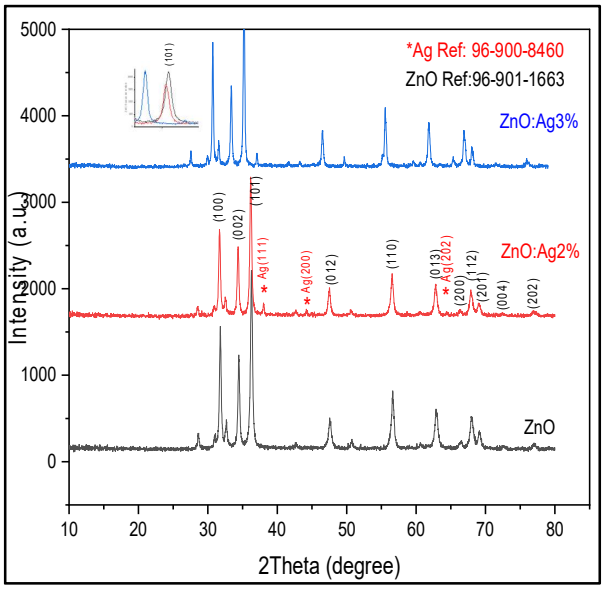

Figure 1B. **XRD pattern of ZnO and Ag-doped ZnO with Reference number**

Distinct peaks that match ZnO's hexagonal wurtzite crystal structure (JCPDS No. (96-901-1663). The hexagonal structure of wurtzite is preserved after Ag doping in the ZnO crystal lattice. The shift of X-ray diffraction peaks is attributed to Ag ion doping and internal tension in the grid in ZnO nanocrystals [24]. Fig 1B displays the X-ray diffraction (XRD) pattern of Ag/ZnO. Furthermore, alongside the diffraction peaks of ZnO, there are additional peaks observed at 38.02, 44.23, 64.63 degrees for Ag/ZnO 2% and 37.02, 43,32, 63.54 degrees for Ag/ZnO 3%. These peaks can be attributed to the (111), (200), and (220) reflections of Ag, respectively. When Ag^{+} is added to ZnO, the peak moves to a lower angle than when ZnO is present alone.

Since we doped the Ag into ZnO, it exhibits a secondary phase transformation corresponding to the (111), (200), and (220) planes (JCPDS card no. 040783) with an FCC lattice. In the XRD diagram of Ag-doped ZnO, we observed a little shift in the position of the (002) and (101) peaks towards smaller angles for ZnO:Ag 2%. In a similar vein, diffraction peak intensity increases and peak straightens with increased silver doping. Whereas for the 3% one, there is a more pronounced shift with an increase in the crystallinity of the peaks. The result is that as the amount of silver doping increases, the crystalline structure of the produced nanoparticles increases. Zn sites are replaced with silver ions, as seen by the shifting positions of the favourably suited crystalline planes (002) and (101) in the ZnO:Ag 2% sample. Because the ionic radii of silver and zinc ions differ, and silver ions have higher ionic radii than zinc ions in the ZnO:Ag 3% sample, the alteration of the peaks may be attributable to this fluctuation rather than the weight percentage of doped silver. Because silver and zinc had very different ionic radii, the exchange of Ag with Zn sites was difficult.

As an alternative, silver ions entangle with ZnO's surface.

The average crystallite size of ZnO alone and doped was calculated from the DRX using the Scherrer formula [25].

$$D_c = \frac{K\lambda}{\beta cos\theta}$$

Where K = 0.89 (a constant), θ (the Bragg's angle), β (the full width at half maximum, or FWHM) of the selected XRD peak, and θ (the diffraction angle) indicate the wavelength of the X-ray. Using the Scherrer equation, the crystal sizes of ZnO and ZnO:Ag 2% and ZnO:Ag 3% NPs have been calculated, and they are 28,517, 26,063, and 37.968 nm, respectively. Crystallite size calculated using a Williamson-hall plot of ZnO and ZnO:Ag 2% and ZnO:Ag 3% NPs are 20.4, 37nm, and 73nm, respectively.

By the Williamson-Hall method, the crystallites of the ZnO NPs 20.4 nm are reduced compared to those obtained by the Scherer equation 28.52 nm.

For ZnO:Ag 2% Williamson-Hall method gives a larger size (37 nm) compared to the Scherer equation (26.06 nm). From ZnO:Ag 3%, a significant increase was observed using the Williamson-Hall method (73 nm) compared to the Scherer equation (37.97 nm). The SEM image Fig. 2 revealed that Ag was a spherical nanoparticle, and ZnO was in the spherical form, has a 45–76 nm average particle size. EDX Fig. 3 examined the chemical components of the produced nanoparticles, revealing the presence of Zn, O, and Ag atoms, indicating their high purity. Table 1 presents the atomic percentages of each element. These results show that the Ag-doped ZnO contains appropriate amounts of Ag, Zn, and O in the sample. The optical bandgap energy (Eg) of the synthesized samples can be calculated by Tauc's method [26, 30]. Ag-doped ZnO NPs exhibit an optical bandgap energy ranging from 3.41 eV for ZnO:Ag 2% (Fig. 4A) and 3.162 eV for ZnO:Ag 3% (Fig.4B), which are lower than 3.54 eV for the bandgap of ZnO nanoparticles Fig.4C. The band gap energy of ZnO is decreased for Ag-doped ZnO, indicating the impact of silver doping on the band-gap energy.

The findings of this investigation are compiled in Table 2, which also contrasts them with data on the environmentally friendly production of Ag–ZnO NPs that have already been published. Table 3 compared the photocatalytic efficacy of the nanoparticles produced in this study with those previously reported for the degradation of the same dye (methylene blue).

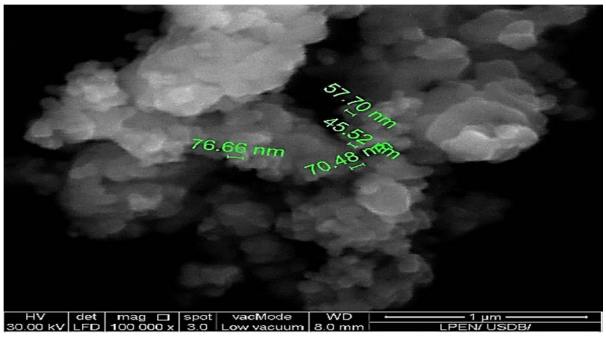

Figure 2. **SEM micrograph of 2 wt% Ag-doped ZnO-NPs using aqueous extract of melon peels**

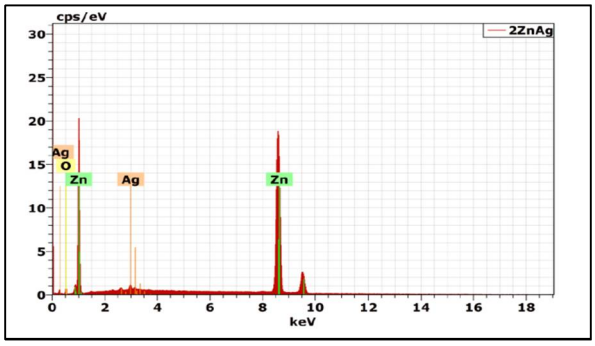

Figure 3. **EDX image of synthesized doped ZnO:Ag 2% NPs using aqueous extract of melon peels**

Table 1. **Atomic percentages of Elements.**

Element	Weight %	Atomic %
Ag	2.41	1.35
Zn	94.64	87.48
O	2.96	11.18

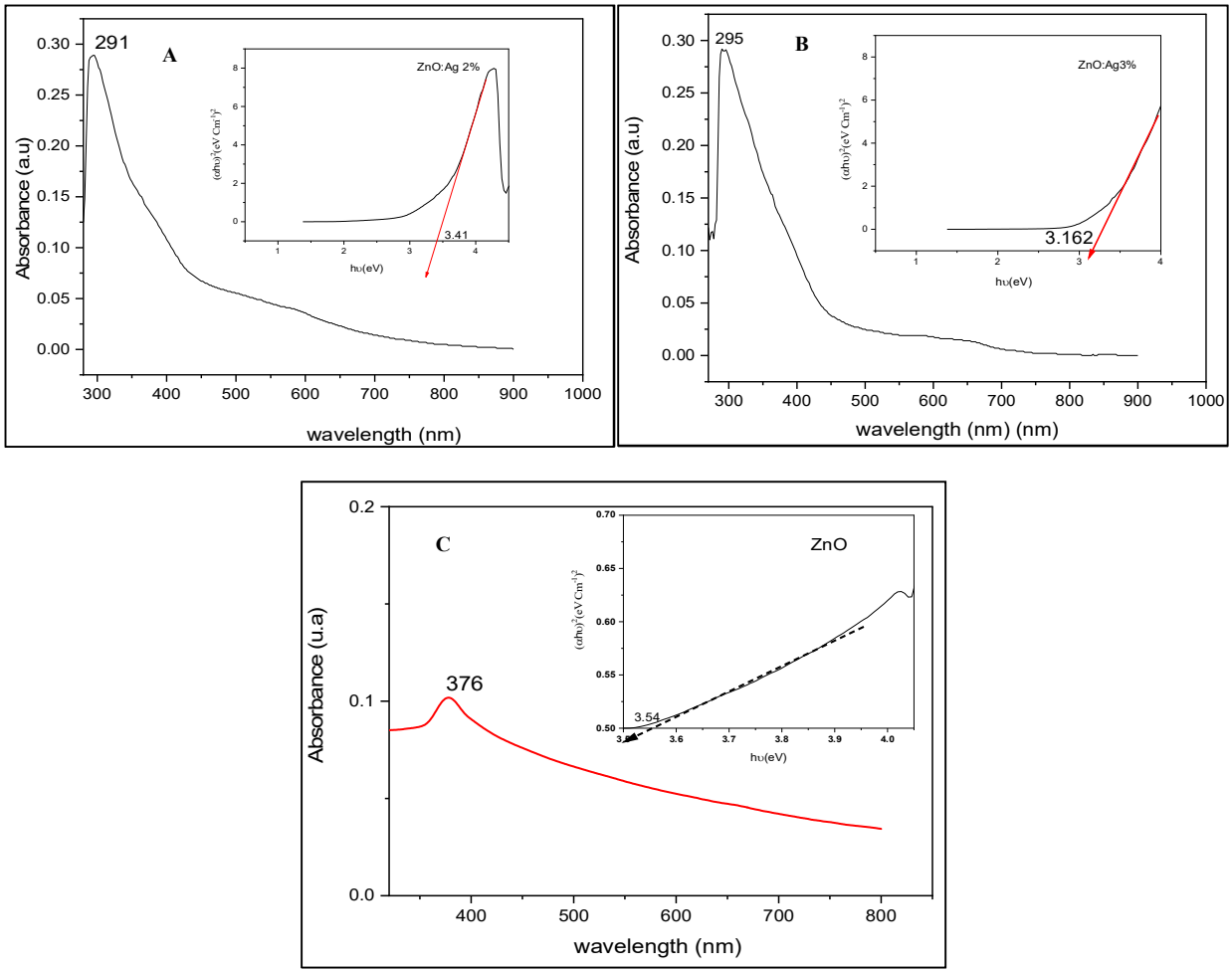

Figure 4. **Estimation of band-gap energy for A=ZnO, B=ZnO doped 2% Ag, and C= ZnO doped 3% Ag photocatalysts**

Table 2. **Comparison of results with published data: Green synthesis of Ag–ZnO nanoparticles.**

Synthesis method	Plant Extract	Crystallite Size	Morphology	Application	Dye	Ref
Reflux method	Ficusbenghalensis	53 nm	Small particles on the larger clusters	*Photocatalytic activity* Antibacterial Activity:	Crystal violet dye	[18]
Co-precipitation method	Aqueous leaf extract of Plectranthusbarbatus	4.419 nm	Irregular shapes and existed in an agglomerated structure	*Antibacterial Activity*	No dye was used.	[26]
Co-precipitation method	Sylvestre leaves	42 nm and 32 nm	Spherical	Antimicrobial activity	No dye was used.	[27]
Hydrothermal method	Neem leaf extracts	21.22 nm and 23.52 nm	Spherical Ag NPs on the surface of ZnO	Optical, and electrical properties	No dye was used.	[28]
Hydrothermal method.	Trigonellafoenum - graecum leaf	75 nm	Ag spherical and fine NPs and ZnONPs rods and plates	Antioxidant activity Antibacterial and antifungal activity Photocatalytic activity	Malachite green dye	[29]
Co-precipitation method	Extract of melon peels	26.063 nm	Spherical nanoparticle	Photocatalytic activity *Antibacterial Activity*	methylene blue .	Present Work

Table 3. **Efficiency of prepared nanoparticles compared with previously reported nanoparticles for MB dye.**

% doping	Light source	Degradation efficiency (%)	Degradation time (min)	Ref
2%	Visible	84	30	[16]
4% Ag:ZnO film	Ultra-violet	60.98	120	[30]
2%	Visible light	40	180	[31]
3.3%	Visible light	64	180	[31]
2%	Ultra-violet	85.5	180	This work

Antibacterial Activity

The antibacterial activity of ZnO nanoparticles showed significant inhibition against the tested pathogens (Fig. 5A), while that of ZnO:Ag 2% nanoparticles exhibited a stronger inhibitory effect (Fig. 5B). The measured inhibition zone is shown in Table 4 and Fig. 6. The highest inhibition was observed for ZnO NPs against *E. coli* (23 mm) followed by *S. aureus* (21.5 mm), and *B. cereus* (13.5 mm). Also, the results confirm that the diameter of the inhibitory zones increases with the increase in the concentration of nanoparticles for all the selected strains. Furthermore, it was shown that the antimicrobial activity of ZnO NPs depended on the nature of the interfacial interaction between the NPs and the cell membrane, as well as the type of bacteria considered [32]. According to a recent report by Xiu et al. [33] ZnO NPS have the ability to interact with membrane lipids and cause structural disorder in the membrane, which leads to a loss of the membrane's integrity and ultimately bacterial death. While the antibacterial activity test of ZnO nanoparticles doped with Ag presented in Fig. 7 and Table 5 confirms that the doped nanoparticles have a significant inhibitory effect against the *S.aureus* strain (27.75 mm), followed by *Bacillus cereus* (21 mm) and *E. coli* (18 mm).

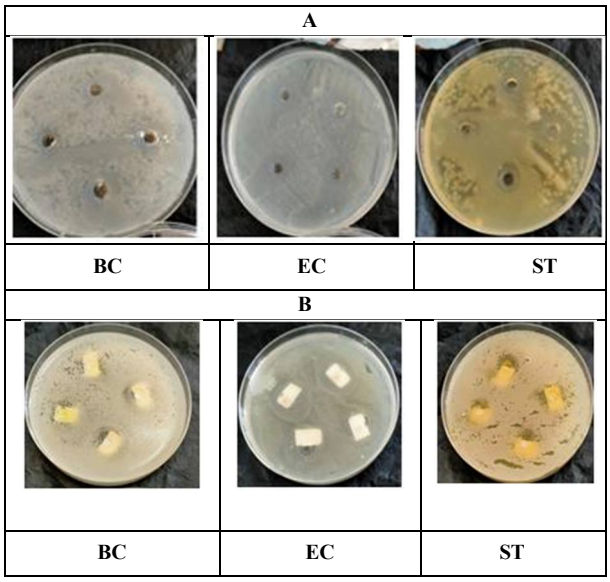

Figure 5. **A= Results of the antibacterial activity of ZnO B= Results of the antibacterial activity of ZnO:Ag 2%**

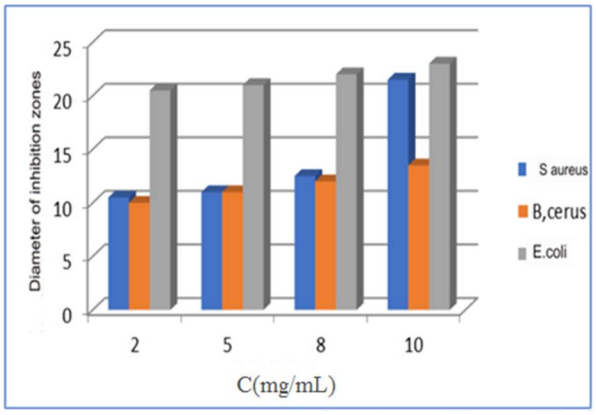

Figure 6. **The inhibitory effect observed on the growth of bacteria by ZnO**

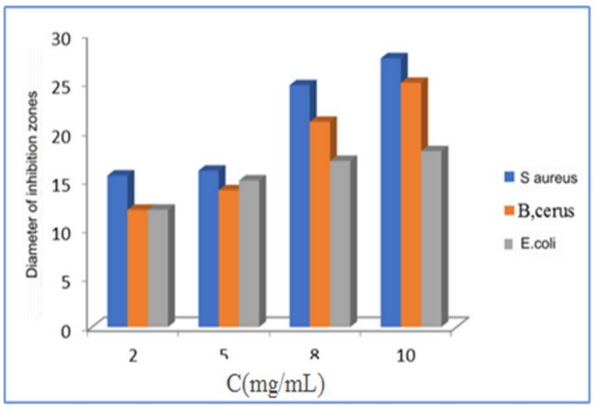

Figure 7. **The inhibitory effect observed on the growth of bacteria by ZnO:Ag 2%**

Table 4. **Zone of inhibition of ZnONPs against bacterial strains**

Microorganism	ZnO NPs			
	2 (mg/mL)	5 (mg/mL)	8 (mg/mL)	10 (mg/mL)
Staphylococcus aureus	10.5	11	12.5	21.5
Escherichia coli	20.5	21	22	23
Bacillus cerus	10	11	12	13.5

Table 5. **Zone of inhibition of ZnO:Ag 2% NPs against bacterial strains.**

Microorganism	ZnO:Ag 2% NPs			
	2 (mg/mL)	5 (mg/mL)	8 (mg/mL)	10 (mg/mL)
Staphylococcus aureus	15.5	16	24.75	27.5
Escherichia coli	12	15	17	18
Bacillus cerus	15	17.25	18.5	21

Photocatalytic analysis

The results in Fig. 8 show that ZnO doped with 2% Ag exhibits a high BM degradation efficiency of 85.03%, while ZnO doped with 3% Ag displays a markedly lower efficiency of 62.24%. These results suggest that 2% Ag represents the optimal doping concentration, as excessive Ag loading may introduce recombination centers for photogenerated charge carriers, thereby reducing photocatalytic activity.

As pH >pHzpc, the surface of ZnO-Ag is weakly negative. Since MB is a cationic dye, its adsorption is favored by the electrostatic interaction with the catalyst surface. This initial adsorption facilitates photodegradation by a better interaction with the active sites of ZnO-Ag. When the catalyst and pollutant are left in contact in the dark, the absorbance measurement is 0.7604. The pollutant shows quick absorption behavior toward the catalyst material. The measurement absorbance reached 0.4562 after 30 minutes, indicating the beginning of the degradation of BM. A rapid degradation is observed in the first 60 min, followed by a slower phase after 90 min, and possible saturation of the active sites or limitation by diffusion. Once the degradation is activated under UV, the reaction follows first-order kinetics, with a rate constant of 0.0072 min^{-1}. The final degradation rate: 85.5% in 180 minOwer catalyst (ZnO doped with 2% Ag). Table 3 under UV achieves 85.5% degradation in 180 min, outperforming the 4% Ag:ZnO film (60.98% in 120 min) [30].

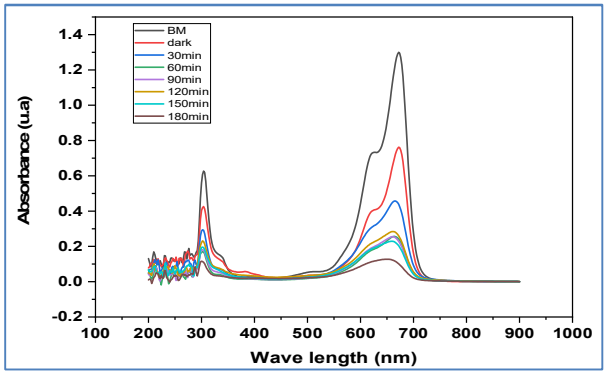

Figure 8. **Absorption spectra of MB solution (10 mg/L) in the presence of 5mg of ZnO:Ag 2%, photocatalyst**

Conclusion

The present study synthesized ZnO and ZnO:Ag (2%) nanoparticles using melon peel aqueous extract and the chemical coprecipitation method. Structural characterization confirmed a hexagonal crystal

structure for all samples. FT-IR spectra validated the presence of Zn–O and Ag bonds, while SEM images revealed that Ag nanoparticles exhibited a predominantly spherical morphology. EDX analysis indicated variations in the expected elemental composition. The green-synthesized ZnO and ZnO:Ag (2%) nanoparticles showed significant antibacterial activity against three pathogenic strains: *Staphylococcus*, *Bacillus cereus*, and *Escherichia coli*. Furthermore, photocatalytic tests demonstrated that ZnO:Ag (2%) nanoparticles achieved 85% degradation of methylene blue.

Conflict of interest

The authors disclosed no conflict of interest.

References

1. G. Applerot, A. Lipovsky, A. Dror, N. Perkas, Y. Nitzan, R. Lubart and A. Gedanken, *Adv. Funct. Mater.,* 19 (2009) 842. https://doi.org/10.1002/adfm.200801081
2. D. Sharma, J. Rajput, B. S. Kaith, M. Kaur and S. Sharma, *Thin Solid Films,* 519 (2010) 1224. https://doi.org/10.1016/j.tsf.2010.08.073
3. A.V. Kirthi, A. Rahuman, G. Rajakumar, S. Marimuthu, T. Santhoshkumar and C. Jayaseelan, *Parasitol. Res.,* 109 (2011) 461. https://doi.org/10.1007/s00436-011-2277-8
4. N. Bala, S. Saha, M. Chakraborty, M. Maiti, S. Das, R. Basuand P. Nandy, *RSC Adv.,* 5 (2015) 4993. https://doi.org/10.1039/C4RA12784F
5. P. Rajiv, S. Rajeshwari and R. Venckatesh, *Spectrochim. Acta A: Mol. Biomol. Spectrosc.,* 112 (2013) 384. https://doi.org/10.1016/j.saa.2013.04.072
6. T. Bhuyan, K. Mishra, M. Khanuja, R. Prasad and A. Varma, *Mater. Sci. Semicond. Process.,* 32 (2015) 55. https://doi.org/10.1016/j.mssp.2014.12.053
7. B.A. Fahimmunisha, R. Ishwarya, M.S. Alsalhi, S. Devanesan, M. Govindarajan and B. Vaseeharan, *J. Drug Deliv. Sci. Technol.,* 55 (2020) 101465. https://doi.org/10.1016/j.jddst.2019.101465
8. M. N. Alharthi, I. Ismail, S. Bellucci, N. H. Khdary and M. Abdel Salam, *Nanomaterials,* 11 (2021) 1682. https://doi.org/10.3390/nano110716822
9. Z. S. Keskin and U. Açıkel, *Cumhur. Sci. J.,* 44 (2023) 90. https://doi.org/10.17776/csj.122335710
10. P. Basnet, T. L. Chanu, D. Samantaand S. Chatterjee, *Photochem. Photobiol. B,* 183 (2018) 201. https://doi.org/10.1016/j.jphotobiol.2018.04.036
11. L. M. Sari and Y. Rilda, *Chem. Sci. Int. J.,* 32 (2023) 1. https://doi.org/10.9734/csji/2023/v32i4850
12. D. Zewde and B. Geremew, *Environ. Pollut. Bioavailab.,* 34 (2022) 224. https://doi.org/10.1080/26395940.2022.2081261
13. F. K. Rhamdiyah and D.K. Maharani, *Indones. J. Chem. Sci.,* 11 (2022) 91. https://doi.org/10.15294/ijcs.v11i2.52498
14. S. Cui, Y. Wu, Z. Cui, P. He, N. Huang, W. Xuand J. Hu, *Mater. Lett.,* 341 (2023) 134158. https://doi.org/10.1016/j.matlet.2023.134158
15. R. Ebrahimi, K. Hossienzadeh, A. Maleki, R.Ghanbari, R. Rezaee, M. Safari and S.H. Puttaiah, *J. Environ. Health Sci. Eng.,* 17 (2019) 479. https://doi.org/10.1007/s40201-019-00366-x

16. S. S. Wagh, V. S. Kadam, C. V. Jagtap, D. B. Salunkhe, R. S. Patil, H. M. Pathan and S. P. Patole, *ACS Omega,* 8 (2023) 7779. https://doi.org/10.1021/acsomega.2c07499
17. D. Blažeka, R. Radičić, D. Maletić, S. Živković, M. Momčilović and N. Krstulović, *Nanomaterials,* 12 (2022) 2677. https://doi.org/10.3390/nano12152677
18. M. C. Shankari, M. Gowri and B. Kavitha, *J. Chem. Environ.,* 27 (2023) 34. https://doi.org/10.25303/2703rjce034046
19. A. Bhosale, J. Kadam, T. Gade, K. Sonawane and K. Garadkar, *J. Indian Chem. Soc.,* 100 (2023) 100920. https://doi.org/10.1016/j.jics.2023.100920
20. A. El Moussaoui, F.Z. Jawhari, A.M. Almehdi, H. Elmsellem, K. F. Benbrahim, D. Bousta and A. Bari, *Bioorg. Chem.,* 93 (2019) 103337. https://doi.org/10.1016/j.bioorg.2019.103337
21. T.S. Aldeen, H.E. A. Mohamed and M. Maaza, *J. Phys. Chem. Solids,* 160 (2022) 110313. https://doi.org/10.1016/j.jpcs.2021.110313
22. A. Fouda, E. Saied, A.M. Eid, F. Kouadri, A.M. Alemam, M.F. Hamza and S.E.D. Hassan, *J. Funct. Biomater.,* 14 (2023) 205. https://doi.org/10.3390/jfb14040205
23. H. Shah, B.A.M. Manikandan and V. Ganesan, *J. Nanomed. Nanotechnol.,* 4 (2017) 03. https://doi.org/10.4172/2157-7439.1000168
24. Y.W. Song, K. Kim, J.P. Ahn, G. Jeang and S.Y. Lee, *Nanotechnology,* 20 (2009) 275606. https://doi.org/10.1088/0957-4484/20/27/275606
25. K. Khormali, Z.M. Mizwari, S.M. Ghoreishi, S. Mortazavi-Derazkola and B. Khezri, *Bioorg. Chem.,* 115 (2021) 105204. https://doi.org/10.1016/j.bioorg.2021.105204
26. A. Alnehia, A. Al-Sharabi, A. Al-Hammadi, A. Al-Odayni, W. S. Saeed and A. Alrahlah, *J. Chem.,* 2023 (2023) 1. https://doi.org/10.1155/2023/1399703
27. P. Vijayakumar, A. J. Ahamed, A. Ravikumar and B. Ragavi, *J. Adv. Appl. Sci. Res.,* 4 (2022) 1. https://doi.org/10.46947/joaasr432022238
28. S. Slathia, T. Gupta and R. P. Chauhan, *Phys. B Condens. Matter.,* 621 (2021) 413287. https://doi.org/10.1016/j.physb.2021.413287
29. Z. Noohpisheh, H. Amiri, S. Farhadi and A. Mohammadi-Gholami, *Spectrochim. Acta A: Mol. Biomol. Spectrosc.,* 240 (2020) 118595. https://doi.org/10.1016/j.saa.2020.118595
30. A.S. Rini, A. P. Defti, R. Dewi and Y. Rati, *Mater. Today Proc.,* 87 (2023) 234. https://doi.org/10.1016/j.matpr.2023.03.100
31. X. Zhang, Y. Wang, F. Hou, H. Li, Y. Yang, X. Zhang and Y. Wang, *Appl. Surf. Sci.,* 391 (2017) 476. https://doi.org/10.1016/j.apsusc.2016.06.109
32. A. S. Karakoti, L. Hench and S. Seal, *JOM,* 58 (2006) 77. https://doi.org/10.1007/s11837-006-0147-0
33. Z.M. Xiu, Q.B. Zhang, H.L. Puppala, V. L. Colvin and P.J. Alvarez, *Nano Lett.,* 12 (2012) 4271. https://doi.org/10.1021/nl301934w